Nano Research
2020, 13(10): 2741–2748
ISSN 1998-0124 CN 11-5974/O4
https://doi.org/10.1007/s12274-020-2921-7

Research Article

Enhancing through-plane thermal conductivity of fluoropolymer composite by developing *in situ* nano-urethane linkage at graphene–graphene interface

Muhammad Maqbool[1], Haichang Guo[1], Akbar Bashir[1], Ali Usman[1], Adeel Y. Abid[1], Guansong He[2], Yanjuan Ren[1], Zeeshan Ali[1,3], and Shulin Bai[1] (✉)

[1] *Department of Materials Science and Engineering, Key Laboratory of High Eenergy Density Physics Simulation (HEDPS)/Center of Applied Physics and Technology (CAPT)/Laboratory of Turbulence and Complex System (LTCS), Key Laboratory of Polymer Chemistry and Physics of Ministry of Education, College of Engineering, Peking University, Beijing 100871, China*
[2] *Institute of Chemical Materials, Chinese Academy of Engineering Physics (CAEP), Mianyang 621900, China*
[3] *School of Chemical and Materials Engineering (SCME), National University of Sciences and Technology (NUST), Islamabad 44000, Pakistan*

Received: 2 January 2020 / **Revised:** 2 June 2020 / **Accepted:** 6 June 2020

ABSTRACT

Attributed to the intense development and complexity in electronic devices, energy dissipation is becoming more essential nowadays. The carbonaceous materials particularly graphene (Gr)-based thermal interface materials (TIMs) are exceptional in heat management. However, because of the anisotropic behavior of Gr in composites, the TIMs having outstanding through-plane thermal conductivity ($^{\perp}$TC) are needed to fulfill the upcoming innovation in numerous devices. In order to achieve this, herein, nano-urethane linkage-based modified Gr and carbon fibers architecture termed as nanourethane linkage (NUL)-Gr/carbon fibers (CFs) is fabricated. Wherein, toluene diisocyanate is utilized to develop a novel but simple NUL to shape a new interface between graphene sheets. Interestingly, the prepared composite of NUL-Gr/CFs with polyvinylidene fluoride matrix shows outstanding performance in heat management. Owing to the unique structure of NUL-Gr/CFs, an unprecedented value of $^{\perp}$TC (~ 7.96 W·m^{-1}·K^{-1}) is achieved at a low filler fraction of 13.8 wt.% which translates into an improvement of ~ 3,980% of pristine polymer. The achieved outcomes elucidate the significance of the covalent interaction between graphene sheets as well as strong bonding among graphene and matrix in the composites and manifest the potential of proposed NUL-Gr/CFs architecture for practical applications.

KEYWORDS

graphene, thermal interface materials, polymer composites

1 Introduction

According to Moore's law, the speed and complexity of electronic devices can be expected to double every two years [1]. Thereby, energy dissipation is becoming a vital and obligatory issue resulting in the reduction of their lifespan for the last few decades [2–11]. To enhance the lifecycle of these substantial devices, to name a few are, solar cell [12], light-emitting diodes [13] and batteries [14–17], thermally conductive materials such as thermal interface materials (TIMs) [18], phase change materials (PCMs) [19], thermal grease, and thermal pads have been utilized as a heat spreader [4, 19–21]. However, the tailorable properties of polymer based TIMs make them exceptional in heat management. Generally, among a bunch of thermally conductive fillers, the carbonaceous material particularly single/few layer graphene (Gr) shows a very high thermal conductivity (TC) range of 3,000–5,500 W·m^{-1}·K^{-1} [22]. Owing to its extraordinary thermal conductance, any suitable substitute has still not been reported. Therefore, researchers are still trying to employ it in making polymer-based TIMs in different ways to acquire acceptable TC values ranging from 4–10 W·m^{-1}·K^{-1} [23]. In contrast, due to entangled molecular chains and amorphous nature, polymers exhibit very low TC (< 0.5 W·m^{-1}·K^{-1}). Besides, the flexibility of TIMs is a remarkable objective which also helps to cover 100% contact between the electronic chip and heat sink at normal pressure [24, 25]. Contrary, the poor mechanical properties give rise to micro-cracks having TC of 0.032 W·m^{-1}·K^{-1} which dramatically suppresses the performance of TIMs [23, 26]. While fabricating polymer-based TIMs, usually, higher TC can be achieved by increasing filler concentration (> 20 wt.%), thus resulting in atrocious mechanical properties. Hence, the adoption of a unique methodology is essential that can provide a serious breakthrough in developing TIMs having high through-plane TC ($^{\perp}$TC) at low fillers contents.

Recently, the high in-plane TC of 1,434 W·m^{-1}·K^{-1} was obtained for layer by layer purely graphene-based film (PGrF), which is much favorable for heat dissipation [27, 28]. Due to extraordinary mass production, it has been used a lot for making portable devices and electronics. Although these values are very high however, $^{\perp}$TC is very low ranging from 0.1–3.4 W·m^{-1}·K^{-1} [29–31]. Planer hexagon of sp^2 carbon in Gr easily realizes this

Address correspondence to slbai@pku.edu.cn

value, if we talk about $^{\perp}$TC, van der Waals interactions play an opposite role because it is not that easy for phonon to travel through highly stacked Gr sheets or through physical bonding [32, 33]. In order to improve $^{\perp}$TC in PGrF, Zhang et al. reported three dimensional (3D) bridged carbon-nanoring (CNR)/Gr hybrid wherein CNR is attached with Gr by covalent bond [34]. However, improved $^{\perp}$TC is still very low. In addition, PGrF is also not enough flexible. Attributed to outstanding flexibility of polymers, nowadays Gr-based polymer composites as TIMs are widely explored. In a very recent study, Barani et al. reported epoxy-based graphene and copper hybrid composite wherein the highest $^{\perp}$TC of 13.5 W·m^{-1}·K^{-1} at 75 wt.% fillers loading was recorded [6]. Since phonons travel through chemical bonds, when they try to go through entangled chains more and more phonon scatters due to the short mean free path of phonons (MFP). Also, it is very hard for a phonon to cross the interface of Gr-polymer [35, 36]. To avoid interface related problems, Song et al. investigated a bridge type effect of SiC among Gr sheets through a melt mixing technique [37]. It is reported in this study, that after adding 43.2 wt.% SiC in 2 wt.% Gr-based polyamide 6 (PA6) composite, $^{\perp}$TC enhancement reaches to 199% of that composite. Consequently, these values at very high filler loading still could not contest the above criteria of acceptable TC range as well as gave inferior mechanical properties.

In this article, we aim to satisfy the upcoming demand of TIMs related challenges. According to the appeal of $^{\perp}$TC in polymer composites, a two-step industrial approach is adopted to fabricate multiple fillers containing polymer composites. Firstly, toluene diisocyanate (TDI) is employed to develop nanourethane linkage (NUL) between graphene sheets and then fastened them again by carbon fibers (CFs) to attain unique 3D-architecture (NUL-Gr/CFs) for the fabrication of polyvinylidene fluoride-based composite. Results inveterate covalent, van der Waals, and hydrogen bonding within the composites, thus forming better conductive paths for phonons transportation. Optimized composites obtained through this strategy achieved a very high $^{\perp}$TC of 7.96 W·m^{-1}·K^{-1} at just 13.8 wt.% filler loading. Nevertheless, electrical conductivity and ion diffusion capabilities are also analyzed, exposing the exceptionality of this functionalization method. The proposed strategy is strongly expected to bring a positive change in polymer composite-based TIMs and open up some new gateways for upcoming researchers.

2 Results and discussions

2.1 Characterization of NUL-Gr

Schematic illustration for the fabrication of NUL-Gr/CFs and NUL-Gr/CFs/polyvinylidene fluoride (PVDF) composite is shown in Fig. 1. Quality of pristine Gr and NUL-Gr is compared with respect to interlayers spacing, number of layers, and defects, etc. as illustrated by transmission electron microscopy (TEM) (Fig. 2). It is evident from Figs. 2(a) and 2(b) that the pristine Gr consists of more than ten layers which also shows consistency with atomic force microscopy (AFM) results presented in Fig. S1 in the electronic supplementary material (ESM). Further, inverse fast Fourier transform (FFT) (inset in Fig. 2(b)) displays that each layer is unglued by 0.35 nm. It is interesting to point out that the isocyanate group of TDI reacts with two Gr sheets resulting in NUL which plays role as a chemical link between them. It is noticed and pointed by black arrows in Figs. 2(c) and 2(f), two Gr sheets are connected by sphere-like bits. These bits having diameter 4–6 nm and showing the interlayer spacing of ~ 0.20 nm (inset in Fig. 2(e)) are clearly

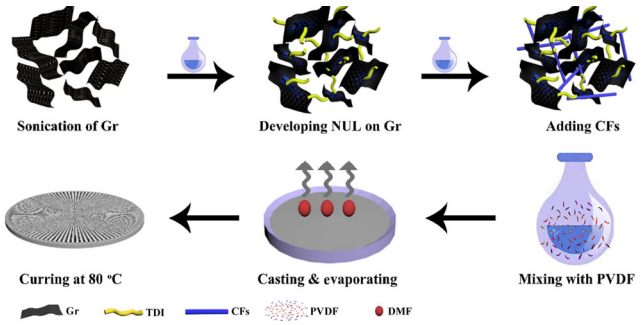

Figure 1 Schematic illustration for the fabrication of NUL-Gr/CFs and NUL-Gr/CFs/polyvinylidene fluoride (PVDF) composite.

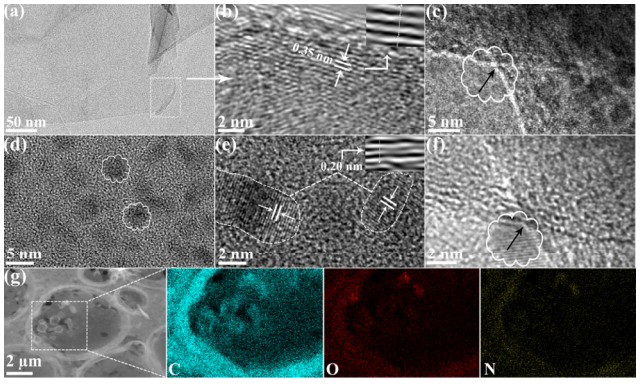

Figure 2 TEM images of Gr and NUL-Gr: (a) and (b) displaying of transparency and more than ten layers in pristine Gr. (c) and (f) Gr sheets connected (black arrows) with each other through NUL in NUL-Gr. (d) and (e) NUL sphere (3–6 nm in diameter) revealing crystallinity. (g) EDS mapping displaying the involvement of nitrogen atom.

representing NUL [38]. Owing to its very small diameter (likewise quantum dots) and partial electronic properties, they are crystalline to some extent (Fig. 2(e) and Fig. S2(d) in the ESM). Indeed, their crystallinity is comparatively better than pristine Gr. Besides, the composition of NUL-Gr is further examined by energy dispersive spectroscopy (EDS) mapping carried out by high- angle annular dark-field (HAADF) detector attached with TEM (Fig. 2(g)). EDS mapping in Fig. 2(g) indicates that the NUL-Gr possesses additional nitrogen atoms whereas pristine Gr only exhibits carbon and oxygen. It is also worth mentioning that after surface treatment of Gr, the quality of NUL-Gr (Fig. S2(f) in the ESM) is found similar to pristine Gr (Fig. 2(b)).

Owing to its bi-functional nature, the TDI molecule can react with two graphene sheets simultaneously, however, it does not affect the whole properties of graphene. This proposition is confirmed by the Fourier transform infrared spectrometer (FTIR) analysis presented in Fig. 3(a). The well-known characteristic peak in TDI at 2,274 cm^{-1} ascribed to NCO group, which reacts with –OH (stretching vibration at 3,464 cm^{-1}) of commercial graphene. Both peaks disappeared while some new peaks at 3,334 and 1,700 cm^{-1} due to N–H and C=O vibration stretching appeared respectively in G-TDI. According to our results and Refs. [19, 38–40], these new peaks confirm the formation of NUL on graphene sheets. Furthermore, the doublet around 2,900 cm^{-1} in G-TDI arises due to the C–H symmetric and asymmetric of the CH_3 group present in TDI. The other distinguished band is observed at 800 cm^{-1} attributing to N–H waging which generally presents in secondary amines, also sometimes in primary amines with other two peaks in the 910–665 cm^{-1} region. Moreover, a relatively prominent band of C–N stretching vibration at 1,300 cm^{-1} than a weaker band at 1,230 cm^{-1} is observed in G-TDI for aromatic and aliphatic

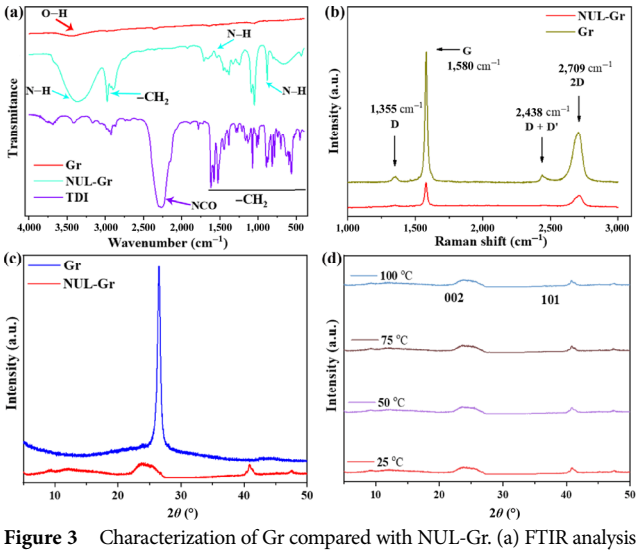

Figure 3 Characterization of Gr compared with NUL-Gr. (a) FTIR analysis showing the appearance of various functional groups on NUL-Gr. (b) Raman spectra displaying minimal D band in NUL-Gr compared with Gr. (c) New X-ray diffraction pattern in NUL-Gr due to the surface treatment of Gr by TDI. (d) Temperature-dependent XRD of NUL-Gr.

amines, respectively. It is to be noted here that a small amount of TDI is utilized because of the fewer number of –OH groups present on graphene. These results summarize that the NCO groups start diminishing, corresponding to the fact that each molecule of TDI (bi-functional) reacts with two graphene sheets simultaneously. In another sense, as the TDI molecule is very small, so one molecule can also react with only one sheet, however commercial grade's graphene sheets are not enough rich in –OH groups. In contrast to this, a large amount of TDI would leave some unreacted NCO groups which may affect the quality of Gr sheets similar to functionalized/oxidized Gr [40].

Raman spectra of pristine Gr and NUL-Gr are shown in Fig. 3(b). The well-recognized characteristic peaks such as D, G, and 2D are witnessed at 1,355, 1,580, and 2,709 cm^{-1} respectively for both Gr and NUL-Gr [41]. As TDI reacts with Gr, the D peak intensity inhibits to some extent because of the decrease in hydroxyl groups related defects which are being fixed by isocyanates [42, 43]. Hence, owing to the specific reactive nature of NCO groups, it is verified again that quality of Gr remains unaffected.

Furthermore, the XRD analysis (Fig. 3(c)) reveals that the pristine Gr exhibits only one sharp diffraction peak at 26.5° for 002 planes of the sp^2-hexagonal structure. On the other hand, two diffractions at 2θ of 24° and 41° are detected for NUL-Gr. More importantly, the diffraction peak of 002 planes is noticed broad and centered at somewhat lower 2θ. According to Refs. [39, 44], the position of urethane linkage's peaks shifts with different types of chain extenders as well as by using various polyols, isocyanate, and salts, etc. However, one thing is common and matching with our results that polyurethane has multiple positional peaks at the above mentioned positions. In addition, the interlayers spacing for Gr and spherical bits (shown in Figs. 2(b) and 2(f)) are confirmed by using brag's law ($\lambda = 2d\sin\theta$). The corresponding d-spacing at 26.5° and 41° is found to be 0.35 and 0.22 nm, respectively, which are also in a close agreement with TEM results. As can be seen in temperature dependent X-ray diffraction (XRD) of NUL-Gr (Fig. 3(d)), the additional peak at 41° is stable up to 100 °C revealing its stability. To reassure, weight loss is also analyzed to investigate the thermal stability of NUL-Gr and NUL-Gr/CFs/PVDF composites (Figs. S3(c) and S3(d) in the ESM). From the results, it is clearly seen that NUL-Gr shows extra weight losses in the range of 260–374 °C as compared to Gr. It is attributed to develop NUL on Gr. On the other hand, the NUL-Gr/CFs/PVDF composites exhibit two-step degradation profile. About 19% and 30% weight losses are observed in the first and second steps respectively for NUL and PVDF segments in composites. Moreover, the amount of char yields at 800 °C for PVDF and its composite (17 wt.%) are 25.2% and 40% respectively which is consistent with our claimed fillers (Gr + CFs) contents. The corresponding heat flows are also exposed as illustrated in Figs. S4(a) and S4(b) in the ESM. Owing to NUL on Gr sheets, an obvious and sharp phase transition is accrued exactly at 324 °C. Moreover, NUL-Gr acts as a nucleating agent thus enhancing the melting point of PVDF, also revealing strong interaction of NUL-Gr with PVDF (Fig. S4(b) in the ESM) [45].

To make it clearer, elemental analysis by using X-ray photoelectron spectrometer (XPS) is also conducted to check the presence of NUL as shown in Fig. 4. The inclusive analysis for each atom is carried out by well-known XPS casa software. In order to use this, all peaks fitting are conceded by keeping line shape "GL (30)" and BG type "Shirley". Consequently, the whole survey (Fig. S3(a) in the ESM) of Gr and NUL-Gr consists of two and three elements, respectively [46]. The atomic percentage (at.%) of all three atoms in NUL-Gr is well quantified as 70.87 at.%, 23.22 at.%, and 5.91 at.% for carbon, nitrogen, and oxygen, respectively. Likewise, the overall nitrogen contents (3.05 at.%) in NUL-Gr are also examined from the C/N ratio between the integrated peak area of C1s and N1s.

To check the bonding behavior of each element, every peak is deconvoluted. A very sharp and intense peaks of C1s at 284.2 and 284.5 eV in full survey (Fig. S3(a) in the ESM) of pristine Gr and NUL-Gr respectively are witnessed into several constituents as shown in Figs. 4(a) and 4(b). One prominent peak in Fig. 4(b) can be clearly observed at 288.7 eV which is well belonging to nitrogen bonded C=O [47]. This peak rose due to the transfer of protons from Gr to NCO groups as mentioned in FTIR. On the other hand, owing to the formation of NUL, a new positional peak for N1s (centered at 400 eV) is also observed in the full survey of NUL-Gr (Fig. S3(a) in the ESM). As this peak is deconvoluted, it comes to know that it belongs to a substance where different bonding behaviors, such

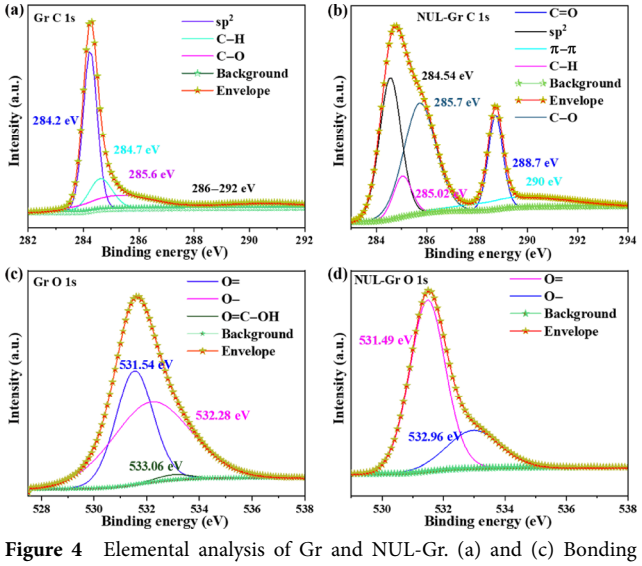

Figure 4 Elemental analysis of Gr and NUL-Gr. (a) and (c) Bonding behavior of C1s and O1s in Gr whereas (b) and (d) in NUL-Gr. The spectrum is deconvoluted into several constituents, such as carbon–carbon bond (sp^2, C–H, C–O, and π–π stacking) and oxygen functional group (O= and O–).

as N–H, N–Csp^2, and N–Csp^3 can be seen (Fig. S4(b) in the ESM) [48]. From the comparison of O1s of both Gr and NUL-Gr, the intensity of peak is increased a lot due to attachments of TDI molecule on the defective surface of Gr (Figs. 4(c) and 4(d)). Therefore, it is concluded from these results and Refs. [47, 49] that NUL is developed, which is consistent with TEM, FTIR, XRD, thermogravimetric analysis (TGA), and differential scanning calorimetry (DSC) outcomes.

The compatibility of Gr and NUL-Gr with PVDF in 5 wt.% composite is visualized by scanning electronic microscopy (SEM). From Figs. 5(b) and 5(c), it is clearly seen that NUL-Gr sheets are well distributed and compatible within the matrix. Contrarily, attributed to its comparatively non-polar nature, the poor distribution and compatibility are observed in case of pristine Gr (Figs. S5(d)–S5(f) in the ESM). Compatibility is assigned to the presence of partially positive charge containing hydrogen atoms in NUL-Gr, which assists in developing strong hydrogen bonding with fluorine atoms of PVDF. The blue color straight line in Fig. 5(d) is displaying the lateral dimension of Gr sheets. Interestingly, besides good compatibility, NUL-Gr sheets are noticed aligned along the vertical direction as can be seen in Fig. 5(c).

For getting it more easily, some additional images are taken from the cross-sectional view of a similar sample as shown in Figs. S5(a)–S5(c) in the ESM. Once again, these sheets are found aligned along the vertical direction (pointed by yellow arrows and dotted lines). Small but straight chains of TDI help Gr sheets to stay connected with each other. This alignment is accrued probably due to bubbles escaping phenomenon (Fig. 6(a)) during the fabrication of composite. In NUL-Gr/CFs/PVDF, owing to the chemical bond (yellow chains in Fig. 6(a)) between two graphene sheets, bubbles of DMF help in aligning them while escaping between two fussed graphene sheets. Besides, generally the solution mixing method for preparing composites does not 100% efficient and leaves some micro-cracks due to uneven solvent evaporation. For managing this, just 1 wt.% CFs having a length of 30 μm is employed as shown in Figs. 5(e) and 5(f). It is seen that long-range CFs are well penetrated as well as cover such type of micro-cracks (Fig. 5(f)) within the composite. Nevertheless, CFs are also showing interactions (pointing with black arrows) with NUL-Gr.

2.2 Thermal and electrical management capability of NUL-Gr/CFs/PVDF composite

The reliable laser flash technique (LFT) is utilized to determine the heat dissipation competencies of prepared materials. As LFT just gives thermal diffusivity (α), other important

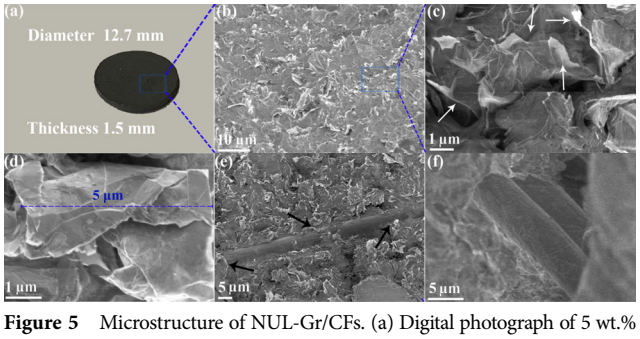

Figure 5 Microstructure of NUL-Gr/CFs. (a) Digital photograph of 5 wt.% NUL-Gr/CFs/PVDF whereas (b) and (c) top view of composite showing well dispersed Gr sheets throughout the matrix wherein white color arrows illustrating vertical alignment to some extent. (d) Demonstrating of the lateral dimension of Gr. (e) and (f) Images demonstrating well penetrated CFs in the matrix and covering micro-air gaps as well as interaction (black arrows) with Gr sheets.

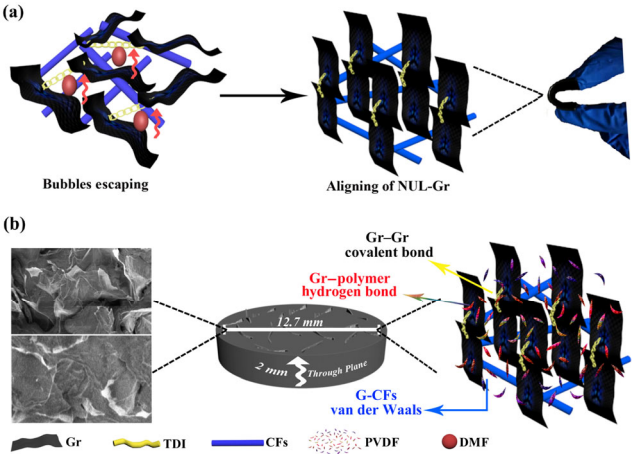

Figure 6 (a) Schematic illustration presenting the alignment of NUL-Gr sheets with bubbles escaping phenomenon. (b) Labeled diagram showing all possible bonding behaviors and interactions of prepared amalgam with the polymer matrix.

parameters, such as heat capacities (C_p) and densities (ρ) of all composites, are also examined (Fig. 7(a) and Table S1 in the ESM). Attributed to high ρ and low C_p of Gr than PVDF, a very common phenomenon, such as an increase in ρ but a decrease in C_p, is observed while increasing Gr contents in composites. To derive $^{\perp}$TC, all parameters are summarized according to a well-known equation (Eq. (1) in Section 4.3). From Fig. 7(b), it is seen that k uniformly increases up to 10 wt.% filler loading and reaches to a relatively low value of 2.2 W·m^{-1}·K^{-1}. However, this loading is not enough for the comprehensive saturation of Gr sheets in a matrix. For better permeation and more connections of Gr sheets with each other, loading is increased up to 17 wt.% wherein an abrupt increase is observed, up to the highest $^{\perp}$TC of ~ 7.96 W·m^{-1}·K^{-1}. These results are further verified by using another reliable instrument, named a trident measurement system. Although 18 wt.% of Gr and CFs were incorporated collectively, however, TDI is applied to decorate nanourethane in NUL-Gr/CFs filler. Hence, according to theoretical calculation and TGA results, total filler fraction (Gr + CFs) in a composite (designated as 17 wt.%) is 13.8 wt.%.

For the sake of convenience, the effect of NUL and CFs is investigated by preparing 5 wt.% composites separately. It is concluded that both NUL [40] and CFs [50] play a positive role in enhancing $^{\perp}$TC (Fig. 7(c)). The NUL helps to decrease weak interfaces such as physical linkages and develop new strong interfaces (covalent bonds). It is already explained in Figs. 2(c) and 2(f) that NUL plays a role of bridge between two Gr sheets which assists in providing suitable paths for phonons. Since NUL is a chemical bond that takes heat from one Gr and transfers through its bond to other Gr sheets. This heat transfer mechanism is very much reported already [8, 51, 52]. When a phonon travels from one part to another, it needs vibration motion of the bonded atom. Chemical bonds offer ease for phonon transfer as compared to physical bonding or nonbonding condition. Although NUL is derived from a sort of polymer which shows poor TC, herein, owing to their fine and crystalline nature, it is providing suitable paths for phonons. Moreover, due to the high compatibility of NUL-Gr with polymer chains, there are quite fewer chances for phonons scattering at matrix–filler interfaces. Contrarily, the pristine Gr shows weak interaction with matrix as well as with other Gr sheets, resulting in scattering of phonons while crossing these interfaces.

Nevertheless, the incorporated CFs behave as 3D architecture developer in NUL-Gr as shown in Figs. 5(e) and 5(f). They

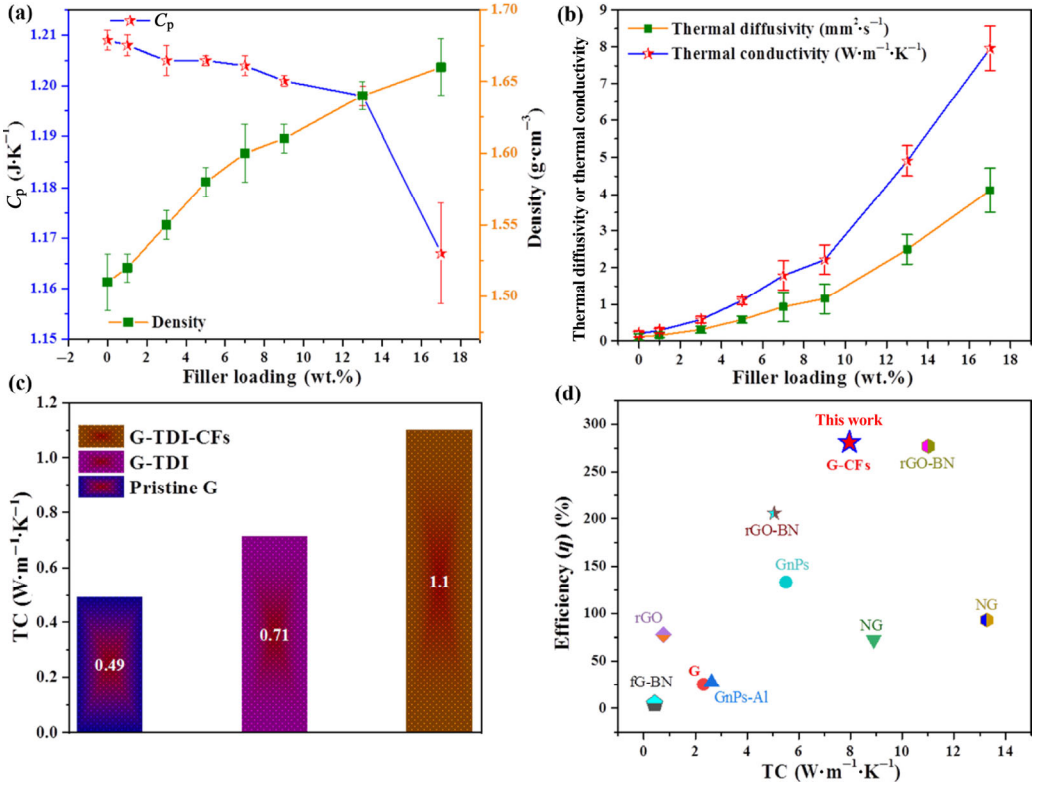

Figure 7 Thermal conduction capability of NUL-Gr/CFs/PVDF. (a) Variation in heat capacity and density as well as (b) thermal diffusivity and thermal conductivity of the corresponding composites. (c) Comparison of $^{\perp}$TC among 5 wt.% pristine Gr, NUL-Gr, and NUL-Gr/CFs composites whereas (d) with published results.

cover micro-cracks which usually generate due to uneven evaporation of solvent while curing of the composite [50]. These micro-cracks significantly hinder the traveling of phonons resulting in a decrease of TC. We emphasize in Fig. 7(c), by adding just 1 wt.% CFs in 5 wt.% NUL-Gr-based PVDF composite, the $^{\perp}$TC is improved from 0.71 to 1.1 W·m^{-1}·K^{-1}. On the other hand, the unprecedented $^{\perp}$TC is also ascribed to already revealed phenomenon in SEM images that NUL-Gr sheets are aligned along the vertical direction [53] as well as connected through covalent bonds. The prepared NUL-Gr/CFs architecture provides continuous conductive paths to phonons in the matrix as illustrated in Fig. 6(b). Moreover, for comparing our results with literature, the efficiency (η) of all composites is calculated by using an equation $\left(\eta = \frac{K_c - K_m}{K_m \times v_f} \times 100\%\right)$ which is provided in Table 1. According to the results, it is concluded that the efficiency of our material is significantly better as compared with the listed outcomes.

The adopted functionalization technique is assumed to be enough specific towards –OH groups of Gr as discussed above, which would not disturb its other properties. However, when it is used as active material in fabricating electrodes for batteries, the result shows that its ions diffusing property is suppressed to some extent. Figure S6(b) in the ESM shows comparative impedance of Gr and NUL-Gr against lithium electrodes while testing their performance in batteries. Consequently, the NUL-Gr offers little high charge resistance of ~ 184.92 Ω compared with pristine Gr (~ 131.2 Ω). This increment is not that so high as for other functionalized Gr. Besides, the electrical resistivity of all composites is tested by using the ST2643 device. From the results in Fig. S6(a) in the ESM, it is interesting to point out that electrical resistivity decreases with increasing Gr contents. Moreover, the percolation threshold at below 5 wt.% indicates a good dispersion of filler in the polymer matrix. Eventually, the adopted technique is quite special which does not disturb the properties of Gr as reported for other functionalization methods [63].

Table 1 Comparison of through-plane thermal conductivity (TC) and η with various carbon-based fillers in fields of thermal management wherein NG, GnPs, Gr, and fG representing natural graphite, graphene nanoplatelets, graphene, and functionalized graphene respectively

Filler	Content (wt.%)	TC (W·m^{-1}·K^{-1})	η (%)	Fabrication method	Ref.
NG	49.30	13.27	93	Two-roll mill	[54]
NG	60	8.9	72.5	Magnetic alignment	[55]
GnPs	25	5.50	133.5	Solution blending	[56]
GnPs-Al	50	2.62	27.1	Solution blending	[57]
Gr	45	2.31	25	Melt blending	[37]
Reduce graphene oxide (rGO)	4.82	0.76	77.8	Solution blending	[58]
rGO	50	0.13		Solution blending	[59]
fG-boron nitride (BN)	25	0.42	4.8	Solution blending	[60]
rGO-BN	13.16 vol.%	5.05	205.5	Ball milling	[61]
rGO-BN	25.4	11.01	277	Solution blending	[62]
NUL-Gr/CFs	13.8	7.96	281	Solution blending	This work

3 Conclusions

In a nut shell, a two-step, unique, and simple functionalization method for incorporating crystalline nanourethane linkage between graphene sheets is developed. We have also fabricated a phonons conductive architecture by assembling NUL-Gr and CFs in fluoropolymer for outstanding thermal management capability. Exclusive thermal reinforcement influences of NUL and CFs within the composites are illuminated. An unprecedented through-plane thermal conductivity ($^{\perp}$TC) up to 7.96 W·m^{-1}·K^{-1} is achieved at just a 13.8 wt.% of filler loading. Besides, electrical resistivity and ion diffusion abilities of NUL-Gr/CFs are also analyzed to demonstrate the versatility of the adopted functionalization. Importantly, this novel approach for fabricating TIMs is reliable enough to improve well-known challenges in heat management. By getting free of the upcoming problem of conventional polymer-based TIMs, our NUL-Gr/CFs/PVDF architecture with characteristically organic arrangement has prodigious potential to be used as ultra-high performance TIMs with decent chemical and thermal stability.

4 Methods and materials

4.1 Materials

PVDF and commercial grade's graphene sheets (Gr) having more than ten layers and thickness ~ 4–10 nm were bought from Beijing Yili Fine Chemical Co. Ltd., China. CFs (T300, length of 30–40 μm and diameter of 2–5 μm) having TC of 5 W·m^{-1}·K^{-1} were supplied by Yanxing Fiber Co. Ltd., China. High quality (~ 99.9% purity) TDI was purchased from Yanshan Co. Ltd., China. To avoid any contamination, the chemicals, such as acetone, ethanol, and distilled water, were used on instant based.

4.2 Preparation of NUL-Gr/CFs and NUL-Gr/CFs/PVDF 3D architecture

Concisely, the calculated percentage of Gr is added in dimethylformamide (DMF) and sonicated for 2 h in burker sonicator having power 1,000 W. Afterward, the considered amount (1.21 mL) of TDI is added dropwise by using a small needle of the syringe and left the whole mixture for another 2 h sonication. The later dispersion is termed as NUL-Gr. After dispersing and making NUL between graphene sheets, these sheets are again strengthened by CFs through van der Waals forces. Finally, after covering the container with polyethylene film, the mixture is transferred on magnetic stirring for 30 min and designated as NUL-Gr/CFs.

Based on solution mixing, a simple but industrial method is adopted to fabricate polymer composite. In brief, the PVDF solution is made by taking 10 g of polymer in DMF with the help of magnetic stirring for 1 h at 60 °C. This clear transparent polymer solution is mixed with an already prepared suspension of NUL-Gr/CFs and again this whole mixture is left for 30 min sonication. Afterward, the mixing is continuing under shear mixing machine for 1 h at 80 °C. To evaporate excessive amount of solvent, the temperature is increased up to 150 °C wherein it turns into a thick (gel-like) paste. Finally, the homogenous film is fabricated by pouring this mixture in a layer by layer manner. Thus the developed film is kept in a vacuum oven at 150 °C for 4 h followed by curing at a reduced temperature (80 °C) for another 24 h. The same protocol is adopted to obtain composites with various loading, such as 1 wt.%, 3 wt.%, 5 wt.%, 7 wt.%, 9 wt.%, 13 wt.%, and 17 wt.%. It is to note here that the amount of TDI and CFs are kept constant in all composites.

4.3 Characterization

Quality of commercial Gr was re-assured by TEM (JEM-2100F, JEOL). The defects, grain boundaries, and graphitization after treatment with TDI were confirmed by Raman spectrometer under the visible wavelength of 532 nm. To evaluate possible elements, such as oxygen, carbon, and nitrogen for pristine and modified Gr, the XPS (Axis Ultra, Kratos Analytical Ltd.) with Al (mono) Kα was used. Further functional group on the surface of Gr and NUL-Gr was verified by FTIR. Crystallinity and phase structure of NUL-Gr were analyzed by powder X-ray diffraction. Thermogravimetric study (TGA-SDTQ600 from TA) was carried out to check the stability of the Gr and weight loss of composites at a heating rate of 10 °C·min^{-1} under both inert and air atmospheres. The dispersion of NUL-Gr/CFs in polymer matrix and morphology of the composites samples were checked by scanning electron microscopy (FE-SEM, S-4800, HITACHI, Japan). Thermal diffusivity (α) at room temperature was measured by a laser flash method (LFA 447, NETZSCH, Germany). Specific heat capacity and different heat flows in the samples were measured by using DSC (Q2000, TA Instruments, America) with heating rate of 5 (°)·min^{-1} in the range of 0 to 40 °C. The density of samples was measured according to Archimedes' principle by using analytical balance (XS204, Mettler-Toledo AG).

After getting all these values, TC was calculated by

$$k = \alpha \times C_p \times \rho \quad (1)$$

where k, α, ρ, and C_p represent thermal conductivity, thermal diffusivity, density, and heat capacity, respectively.

Acknowledgements

This work was supported by the Nature Science Associate Foundation (NSAF) (No. U1730103) and the National Natural Science Foundation of China (NSFC) (No.11672002)

Electronic Supplementary Material: Supplementary material (AFM, TEM, TGA, DSC, and ESM) is available in the online version of this article at https://doi.org/10.1007/s12274-020-2921-7.

References

[1] Moore, A. L.; Shi, L. Emerging challenges and materials for thermal management of electronics. *Mater. Today* **2014**, *17*, 163–174.

[2] Jeon, D.; Kim, S. H.; Choi, W.; Byon, C. An experimental study on the thermal performance of cellulose-graphene-based thermal interface materials. *Int. J. Heat Mass Tran.* **2019**, *132*, 944–951.

[3] Kostarelos, K.; Novoselov, K. S. Graphene devices for life. *Nat. Nanotechnol.* **2014**, *9*, 744–745.

[4] Razeeb, K. M.; Dalton, E.; Cross, G. L. W.; Robinson, A. J. Present and future thermal interface materials for electronic devices. *Int. Mater. Rev.* **2018**, *63*, 1–21.

[5] Dai, W.; Ma, T. F.; Yan, Q. W.; Gao, J. Y.; Tan, X.; Lv, L.; Hou, H.; Wei, Q. P.; Yu, J. H.; Wu, J. B. et al. Metal-level thermally conductive yet soft graphene thermal interface materials. *ACS Nano* **2019**, *13*, 11561–11571.

[6] Barani, Z.; Mohammadzadeh, A.; Geremew, A.; Huang, C. Y.; Coleman, D.; Mangolini, L.; Kargar, F.; Balandin, A. A. Thermal properties of the binary-filler hybrid composites with graphene and copper nanoparticles. *Adv. Funct. Mater.* **2020**, *30*, 1904008.

[7] Bae, S. H.; Kum, H.; Kong, W.; Kim, Y.; Choi, C.; Lee, B.; Lin, P.; Park, Y.; Kim, J. Integration of bulk materials with two-dimensional materials for physical coupling and applications. *Nat. Mater.* **2019**,

18, 550–560.

[8] Yang, H. Y.; Tang, Y. Q.; Yang, P. Factors influencing thermal transport across graphene/metal interfaces with van der Waals interactions. *Nanoscale* **2019**, *11*, 14155–14163.

[9] Zhang, F.; Feng, Y. Y.; Qin, M. M.; Gao, L.; Li, Z. Y.; Zhao, F. L.; Zhang, Z. X.; Lv, F.; Feng, W. Stress controllability in thermal and electrical conductivity of 3D elastic graphene-crosslinked carbon nanotube sponge/polyimide nanocomposite. *Adv. Funct. Mater.* **2019**, *29*, 1901383.

[10] Mahmood, N.; Islam, M.; Hameed, A.; Saeed, S.; Khan, A. N. Polyamide-6-based composites reinforced with pristine or functionalized multi-walled carbon nanotubes produced using melt extrusion technique. *J. Compos. Mater.* **2013**, *48*, 1197–1207.

[11] Wang, H.; Nie, S.; Li, H.; Ali, R.; Fu, J.; Xiong, H. J.; Li, J.; Wu, Z. Q.; Lau, W. M.; Mahmood, N. et al. 3D hollow quasi-graphite capsules/polyaniline hybrid with a high performance for room-temperature ammonia gas sensors. *ACS Sensors* **2019**, *4*, 2343–2350.

[12] Jia, Y.; Cao, A. Y.; Bai, X.; Li, Z.; Zhang, L. H.; Guo, N.; Wei, J. Q.; Wang, K. L.; Zhu, H. W.; Wu, D. H. et al. Achieving high efficiency silicon-carbon nanotube heterojunction solar cells by acid doping. *Nano Lett.* **2011**, *11*, 1901–1905.

[13] Christensen, A.; Graham, S. Thermal effects in packaging high power light emitting diode arrays. *Appl. Therm. Eng.* **2009**, *29*, 364–371.

[14] Aslam, S.; Sagar, R. U. R.; Liu, Y. X.; Anwar, T.; Zhang, L. W.; Zhang, M.; Mahmood, N.; Qiu, Y. J. Graphene decorated polymeric flexible materials for lightweight high areal energy lithium-ion batteries. *Appl. Mater. Today* **2019**, *17*, 123–129.

[15] Jian, X.; Wang, H.; Rao, G. F.; Jiang, L. Y.; Wang, H. N.; Subramaniyam, C. M.; Mahmood, A.; Zhang, W. L.; Xiang, Y.; Dou, S. X. et al. Self-tunable ultrathin carbon nanocups as the electrode material of sodium-ion batteries with unprecedented capacity and stability. *Chem. Eng. J.* **2019**, *364*, 578–588.

[16] Ali, Z.; Asif, M.; Zhang, T.; Huang, X. X.; Hou, Y. L. General approach to produce nanostructured binary transition metal selenides as high-performance sodium ion battery anodes. *Small* **2019**, *15*, 1901995.

[17] Ali, Z.; Zhang, T.; Asif, M.; Zhao, L.; Yu, Y.; Hou, Y. L. Transition metal chalcogenide anodes for sodium storage. *Mater. Today* **2020**, *35*, 131–167.

[18] Ren, Y. J.; Guo, H. C.; Liu, Y. H.; Lv, R. C.; Zhang, Y. F.; Maqbool, M.; Bai, S. L. A trade-off study toward highly thermally conductive and mechanically robust thermoplastic composites by injection moulding. *Compos. Sci. Technol.* **2019**, *183*, 107787.

[19] Aftab, W.; Mahmood, A.; Guo, W. H.; Yousaf, M.; Tabassum, H.; Huang, X. Y.; Liang, Z. B.; Cao, A. Y.; Zou, R. Q. Polyurethane-based flexible and conductive phase change composites for energy conversion and storage. *Energy Storage Mater.* **2019**, *20*, 401–409.

[20] Aftab, W.; Huang, X. Y.; Wu, W. H.; Liang, Z. B.; Mahmood, A.; Zou, R. Q. Nanoconfined phase change materials for thermal energy applications. *Energy Environ. Sci.* **2018**, *11*, 1392–1424.

[21] Ji, C.; Yan, C. Z.; Wang, Y.; Xiong, S. X.; Zhou, F. R.; Li, Y. Y.; Sun, R.; Wong, C. P. Thermal conductivity enhancement of CNT/MoS_2/graphene−epoxy nanocomposites based on structural synergistic effects and interpenetrating network. *Compos. Part B: Eng.* **2019**, *163*, 363–370.

[22] Balandin, A. A.; Ghosh, S.; Bao, W. Z.; Calizo, I.; Teweldebrhan, D.; Miao, F.; Lau, C. N. Superior thermal conductivity of single-layer graphene. *Nano Lett.* **2008**, *8*, 902–907.

[23] Dai, W.; Lv, L.; Lu, J. B.; Hou, H.; Yan, Q. W.; Alam, F. E.; Li, Y. F.; Zeng, X. L.; Yu, J. H.; Wei, Q. P. et al. A paper-like inorganic thermal interface material composed of hierarchically structured graphene/silicon carbide nanorods. *ACS Nano* **2019**, *13*, 1547–1554.

[24] Warzoha, R. J.; Donovan, B. F. High resolution steady-state measurements of thermal contact resistance across thermal interface material junctions. *Rev. Sci. Instrum.* **2017**, *88*, 094901.

[25] Hameed, A.; Islam, M.; ahmad, I.; Mahmood, N.; Saeed, S.; Javed, H. Thermal and mechanical properties of carbon nanotube/epoxy nanocomposites reinforced with pristine and functionalized multiwalled carbon nanotubes. *Polym. Compos.* **2015**, *36*, 1891–1898.

[26] Renteria, J. D.; Ramirez, S.; Malekpour, H.; Alonso, B.; Centeno, A.; Zurutuza, A.; Cocemasov, A. I.; Nika, D. L.; Balandin, A. A. Strongly anisotropic thermal conductivity of free-standing reduced graphene oxide films annealed at high temperature. *Adv. Funct. Mater.* **2015**, *25*, 4664–4672.

[27] Xin, G. Q.; Sun, H. T.; Hu, T.; Fard, H. R.; Sun, X.; Koratkar, N.; Borca-Tasciuc, T.; Lian, J. Large-area freestanding graphene paper for superior thermal management. *Adv. Mater.* **2014**, *26*, 4521–4526.

[28] Shen, B.; Zhai, W. T.; Zheng, W. G. Ultrathin flexible graphene film: An excellent thermal conducting material with efficient EMI shielding. *Adv. Funct. Mater.* **2014**, *24*, 4542–4548.

[29] Kong, Q. Q.; Liu, Z.; Gao, J. G.; Chen, C. M.; Zhang, Q.; Zhou, G. M.; Tao, Z. C.; Zhang, X. H.; Wang, M. Z.; Li, F. et al. Hierarchical graphene-carbon fiber composite paper as a flexible lateral heat spreader. *Adv. Funct. Mater.* **2014**, *24*, 4222–4228.

[30] Jackie, D. R.; Sylvester, R.; Hoda, M.; Beatriz, A.; Alba, C.; Amaia, Z.; Alexandr, I. C.; Denis, L. N.; Balandin, A. A. Strongly anisotropic thermal conductivity of free-standing reduced graphene oxide films annealed at high temperature. *Adv. Funct. Mater.* **2015**, *25*, 4664–4672.

[31] Yim, M. J.; Paik, K. W. Recent advances on anisotropic conductive adhesives (ACAs) for flat panel displays and semiconductor packaging applications. *Int. J. Adhes Adhes.* **2006**, *26*, 304–313.

[32] Meng, X.; Pan, H.; Zhu, C. L.; Chen, Z. X.; Lu, T.; Xu, D.; Li, Y.; Zhu, S. M. Coupled chiral structure in graphene-based film for ultrahigh thermal conductivity in both in-plane and through-plane directions. *ACS Appl. Mater. Interfaces* **2018**, *10*, 22611–22622.

[33] Yousefi, N.; Gudarzi, M. M.; Zheng, Q. B.; Aboutalebi, S. H.; Sharif, F.; Kim, J. K. Self-alignment and high electrical conductivity of ultralarge graphene oxide–polyurethane nanocomposites. *J. Mater. Chem.* **2012**, *22*, 12709–12717.

[34] Zhang, J. W.; Shi, G.; Jiang, C.; Ju, S.; Jiang, D. Z. 3D bridged carbon nanoring/graphene hybrid paper as a high-performance lateral heat spreader. *Small* **2015**, *11*, 6197–6204.

[35] Ronca, S.; Igarashi, T.; Forte, G.; Rastogi, S. Metallic-like thermal conductivity in a lightweight insulator: Solid-state processed ultra high molecular weight polyethylene tapes and films. *Polymer* **2017**, *123*, 203–210.

[36] Zhu, B. W.; Liu, J.; Wang, T. Y.; Han, M.; Valloppilly, S.; Xu, S.; Wang, X. W. Novel polyethylene fibers of very high thermal conductivity enabled by amorphous restructuring. *ACS Omega* **2017**, *2*, 3931–3944.

[37] Song, N.; Pan, H. D.; Hou, X. S.; Cui, S. Q.; Shi, L. Y.; Ding, P. Enhancement of thermal conductivity in polyamide-6/graphene composites via a “bridge effect” of silicon carbide whiskers. *RSC Adv.* **2017**, *7*, 46306–46312.

[38] Morsi, S. M. M.; Mohamed, H. A. A comparative study of new linear and hyperbranched polyurethanes built up from a synthesized isocyanate-terminated polyester/urethane. *Polym. Bull.* **2017**, *74*, 5011–5027.

[39] Oprea, S.; Timpu, D.; Oprea, V. Design-properties relationships of polyurethanes elastomers depending on different chain extenders structures. *J. Polym. Res.* **2019**, *26*, 117.

[40] Wu, S. L.; Shi, T. J.; Zhang, L. Y. Preparation and properties of amine-functionalized reduced graphene oxide/waterborne polyurethane nanocomposites. *High Perform. Polym.* **2015**, *28*, 453–465.

[41] Wu, J. B.; Lin, M. L.; Cong, X.; Liu, H. N.; Tan, P. H. Raman spectroscopy of graphene-based materials and its applications in related devices. *Chem. Soc. Rev.* **2018**, *47*, 1822–1873.

[42] de Leon, A. C.; Alonso, L.; Mangadlao, J. D.; Advincula, R. C.; Pentzer, E. Simultaneous reduction and functionalization of graphene oxide via Ritter reaction. *ACS Appl. Mater. Interfaces* **2017**, *9*, 14265–14272.

[43] Kim, N. H.; Kuila, T.; Lee, J. H. Simultaneous reduction, functionalization and stitching of graphene oxide with ethylenediamine for composites application. *J. Mater. Chem. A* **2013**, *1*, 1349–1358.

[44] Daud, F. N.; Ahmad, A.; Haji Badri, K. An investigation on the properties of palm-based polyurethane solid polymer electrolyte. *Int. J. Polym. Sci.* **2014**, *2014*, Article ID 326716.

[45] Mahmood, N.; Islam, M.; Hameed, A.; Saeed, S. Polyamide 6/multiwalled carbon nanotubes nanocomposites with modified

morphology and thermal properties. *Polymers* **2013**, *5*, 1380–1391.
[46] Jiang, Z. J.; Jiang, Z. Q. Interaction induced high catalytic activities of CoO nanoparticles grown on nitrogen-doped hollow graphene microspheres for oxygen reduction and evolution reactions. *Sci. Rep.* **2016**, *6*, 27081.
[47] Zhou, G. M.; Paek, E.; Hwang, G. S.; Manthiram, A. Long-life Li/polysulphide batteries with high sulphur loading enabled by lightweight three-dimensional nitrogen/sulphur-codoped graphene sponge. *Nat. Commun.* **2015**, *6*, 7760.
[48] Li, W. C.; Cui, J.; Wang, W. W.; Zheng, D. H.; Jia, L. F.; Saeed, S.; Liu, H. D.; Rupp, R.; Kong, Y. F.; Xu, J. J. P-type lithium niobate thin films fabricated by nitrogen-doping. *Materials* **2019**, *12*, 819.
[49] Matsoso, B. J.; Ranganathan, K.; Mutuma, B. K.; Lerotholi, T.; Jones, G.; Coville, N. J. Time-dependent evolution of the nitrogen configurations in N-doped graphene films. *RSC Adv.* **2016**, *6*, 106914–106920.
[50] Zhao, Y. H.; Zhang, Y. F.; Bai, S. L.; Yuan, X. W. Carbon fibre/graphene foam/polymer composites with enhanced mechanical and thermal properties. *Compos. Part B: Eng.* **2016**, *94*, 102–108.
[51] Hyun, S. K.; Ji, U. J.; Hyeseong, L.; Seong, Y. K.; Seong, H. K.; Jaewoo, K.; Yong, C. J.; Beom. J. Y. Thermal management in polymer composites: A review of physical and structural parameters. *Adv. Eng. Mater.* **2018**, *20*, 1800204.
[52] Burger, N.; Laachachi, A.; Ferriol, M.; Lutz, M.; Toniazzo, V.; Ruch, D. Review of thermal conductivity in composites: Mechanisms, parameters and theory. *Prog. Polym. Sci.* **2016**, *61*, 1–28.
[53] Zhang, X. R.; Xie, X. Y.; Cai, X. Z.; Jiang, Z. Y.; Gao, T.; Ren, Y. J.; Hu, J.; Zhang, X. X. Graphene-perfluoroalkoxy nanocomposite with high through-plane thermal conductivity fabricated by hot-pressing. *Nanomaterials (Basel)* **2019**, *9*, 1320.
[54] Feng, C. P.; Bai, L.; Shao, Y.; Bao, R. Y.; Liu, Z. Y.; Yang, M. B.; Chen, J.; Ni, H. Y.; Yang, W. A facile route to fabricate highly anisotropic thermally conductive elastomeric POE/NG composites for thermal management. *Adv. Mater. Interfaces* **2018**, *5*, 1700946.
[55] Chung, S. H.; Kim, H.; Jeong, S. W. Improved thermal conductivity of carbon-based thermal interface materials by high-magnetic-field alignment. *Carbon* **2018**, *140*, 24–29.
[56] Zahid, M.; Masood, M. T.; Athanassiou, A.; Bayer, I. S. Sustainable thermal interface materials from recycled cotton textiles and graphene nanoplatelets. *Appl. Phys. Lett.* **2018**, *113*, 044103.
[57] Tian, X. J.; Itkis, M. E.; Haddon, R. C. Application of hybrid fillers for improving the through-plane heat transport in graphite nanoplatelet-based thermal interface layers. *Sci. Rep.* **2015**, *5*, 13108.
[58] Qin, M. M.; Xu, Y. X.; Cao, R.; Feng, W.; Chen, L. Efficiently controlling the 3D thermal conductivity of a polymer nanocomposite via a hyperelastic double-continuous network of graphene and sponge. *Adv. Funct. Mater.* **2018**, *28*, 1805053.
[59] Yang, W. X.; Zhao, Z. D.; Wu, K.; Huang, R.; Liu, T. Y.; Jiang, H.; Chen, F.; Fu, Q. Ultrathin flexible reduced graphene oxide/cellulose nanofiber composite films with strongly anisotropic thermal conductivity and efficient electromagnetic interference shielding. *J. Mater. Chem. C* **2017**, *5*, 3748–3756.
[60] Su, Z.; Wang, H.; Ye, X. Z.; Tian, K. H.; Huang, W. Q.; Xiao, C.; Tian, X. Y. Enhanced thermal conductivity of functionalized-graphene/boron nitride flexible laminated composite adhesive via a facile latex approach. *Compos. Part A: Appl. Sci. Manuf.* **2017**, *99*, 166–175.
[61] Yao, Y. M.; Sun, J. J.; Zeng, X. L.; Sun, R.; Xu, J. B.; Wong, C. P. Construction of 3D skeleton for polymer composites achieving a high thermal conductivity. *Small* **2018**, *14*, 1704044.
[62] An, F.; Li, X. F.; Min, P.; Li, H. F.; Dai, Z.; Yu, Z. Z. Highly anisotropic graphene/boron nitride hybrid aerogels with long-range ordered architecture and moderate density for highly thermally conductive composites. *Carbon* **2018**, *126*, 119–127.
[63] Georgakilas, V.; Otyepka, M.; Bourlinos, A. B.; Chandra, V.; Kim, N.; Kemp, K. C.; Hobza, P.; Zboril, R.; Kim, K. S. Functionalization of graphene: Covalent and non-covalent approaches, derivatives and applications. *Chem. Rev.* **2012**, *112*, 6156–6214.